SURVEY OF DETECTION METHODS FOR ARTM CPM

Erik Perrins and Michael Rice
Department of Electrical and Computer Engineering
Brigham Young University
Provo, UT 84602
esp@ee.byu.edu, mdr@ee.byu.edu

ABSTRACT

The ARTM Tier-2 waveform, called "ARTM CPM" in IRIG 106-04, has almost three times the spectral efficiency of PCM/FM and approximately the same detection efficiency. The improved spectral efficiency comes at the price of computational complexity in the receiver. The optimum receiver requires 128 real-valued matched filters and keeps track of the waveform state with a trellis of 512 states and 2048 branches. Various complexity reducing techniques are applied and the resulting loss in detection efficiency is quantified. It is shown that the full 512-state trellis is not required to achieve the desired detection efficiency: two different 32-state configurations were found to perform within one tenth of a dB of optimal. Noncoherent techniques are also evaluated. It is shown that the required complexity can be quite large to achieve a respectable detection efficiency. One noncoherent technique performed within 1.9 dB of the optimal with only 64 states, which is significant when considering the additional complexity savings of not having to track the carrier phase.

INTRODUCTION

PCM/FM has been the primary modulation format used in aeronautical telemetry for more than 40 years. During this time, the complexity of the systems that need to be tested has increased dramatically. As a consequence the required data rates for the tests have increased from 100 kbits/sec in the early 1970s to 10-20 Mbit/sec today. This increase has applied tremendous pressure on the spectrum allocated to aeronautical telemetry at L-band (1435 – 1535 MHz), lower S-band (2200 – 2290 MHz), and upper S-band (2310 – 2390 MHz). The situation was further exacerbated in 1997 when the lower portion of upper S-band (2310 to 2360 MHz) was reallocated to digital audio radio and wireless communications services by the FCC in two separate auctions.

In response to these trends, the Advanced Range Telemetry (ARTM) program [1] was launched by the Central Test and Evaluation Investment Program (CTEIP) in 1997 to identify more bandwidth efficient

modulation formats compatible with fully saturated non-linear amplifiers for use in aeronautical telemetry. The goal was to select waveforms that have better spectral efficiency than PCM/FM with the same detection efficiency as PCM/FM. Modulation formats with improved spectral efficiency were selected in two phases. In the first phase, Feher-patented QPSK (FQPSK) [2] was adopted in the IRIG 106-00 standard and a compatible variant of the MIL-STD 188-181 Shaped Offset QPSK (SOQPSK) [3] was adopted in the IRIG 106-04 standard. These two modulation formats, known collectively as "ARTM Tier-1 Waveforms," have twice the spectral efficiency as PCM/FM [4], even when used with non-linear power amplifiers. In the second phase, a two-index 4-ary continuous phase modulation [5], was adopted in the IRIG 106-04 standard under the name "ARTM CPM." This waveform, sometimes referred to as the "ARTM Tier-2" waveform, has almost three times the spectral efficiency as PCM/FM.

The improved spectral efficiency of ARTM CPM comes with a price: increased complexity in the receiver. It will be shown that the optimal detector is a sequence detector that requires 128 real-valued matched filters and keeps track of the waveform state with a trellis of 512 states and 2048 branches. The performance of this detector forms the baseline against which the other detectors are compared. Various complexity reducing techniques are applied to the resulting loss in detection efficiency is quantified. The final result is a series of approximations that trade complexity for detection efficiency.

ARTM CPM SIGNAL MODEL

Continuous-phase modulation, or CPM, is a version of frequency shift keying where the transition from one frequency to another maintains a smooth phase that does not have any discontinuities. The frequency transitions can be filtered to produce a digitally modulated FM signal with constant envelope and desirable spectral properties. The improved bandwidth efficiency comes at the expense of detection efficiency. Thus, CPM offers a rich variety of choices in the trade-off between bandwidth and power.

A CPM modulated carrier may be expressed as

$$s(t) = A\cos\left(\omega_0 t + \phi(t)\right) \tag{1}$$

where the time-varying phase $\phi(t)$ contains the information. A CPM signal can be generated by frequency modulating a pulse train where the data symbols $\alpha_0, \alpha_1, \alpha_2, \ldots$ modulate the amplitude of a *frequency pulse* $f(t)$. In a multiple-index scheme, the FM modulation index applied to each symbol is allowed to vary. In this case, the frequency pulse train may be represented as

$$m(t) = \sum_i 2\pi h_i \alpha_i f(t - iT) \tag{2}$$

where α_i is the i-th data symbol, T is the symbol time (or reciprocal of the symbol rate), $f(t)$ is the frequency pulse, and h_i is the digital modulation index[1] used for the i-th symbol. Since frequency is the

[1]The digital modulation index is defined as the ratio of two times the peak frequency deviation to the symbol rate when area of the frequency pulse is normalized to 1/2.

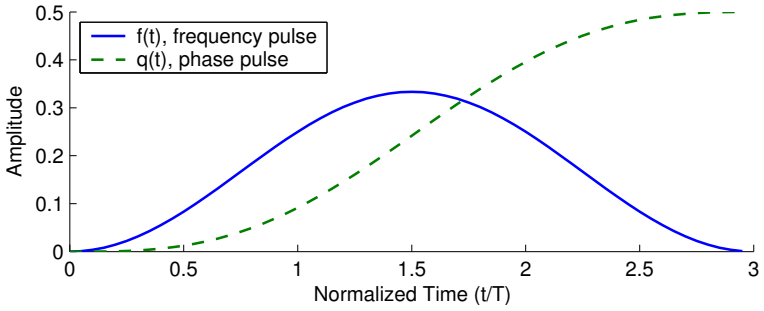

Figure 1: The length-3 raised cosine (3RC) frequency pulse and corresponding phase pulse for ARTM CPM.

Table 1: Parameters defining ARTM CPM.

symbol values	$\alpha_n \in \{-3, -1, +1, +3\}$
partial response	$L = 3$
frequency pulse	$f(t) = \begin{cases} \frac{1}{2LT}\left[1 - \cos\left(\frac{2\pi t}{LT}\right)\right] & 0 \le t \le LT \\ 0 & \text{otherwise} \end{cases}$
modulation indexes	$h_n \in \left\{\frac{4}{16}, \frac{5}{16}\right\}$

time-derivative of phase, the phase $\phi(t)$ in (1) may be expressed as

$$\phi(t) = \int m(x)dx = \sum_i 2\pi h_i \alpha_i \int f(x - iT)dx = \sum_i 2\pi h_i \alpha_i g(t - iT) \tag{3}$$

where $g(t)$ is called the *phase pulse* and has peak amplitude 1/2 when the area of the frequency pulse $f(t)$ is normalized to 1/2. The phase pulse defines the shape of the *phase trajectory* of the modulated carrier. The n-th symbol, α_n forces the phase of the carrier to shift by $\pi h_n \alpha_n$ radians. The phase pulse $g(t)$ defines *how* the phase completes this transition. The instantaneous frequency shift is the time derivative of this transition. By allowing this transition to occur over multiple symbol intervals, the bandwidth of the modulated carrier can be reduced. The frequency pulse $f(t)$ and the corresponding phase pulse $g(t)$ used by ARTM CPM are plotted in Figure 1. Observe that the frequency pulse lasts 3 symbol times. This means that it takes three symbol times for the n-th symbol to shift the carrier phase by $\pi h_n \alpha_n$. The other parameters that define ARTM CPM are listed in Table 1. The two modulation indexes are used in alternation. In the language of CPM, ARTM CPM is a two-index, 4-ary partial response CPM.

During the interval corresponding to the n-th symbol — or equivalently, $nT \le t \le (n+1)T$ — the phase may be expressed as

$$\phi(t) = \sum_{i=0}^{n} 2\pi h_i \alpha_i g(t - iT) = \underbrace{\sum_{i=n-2}^{n} 2\pi h_i \alpha_i g(t - iT)}_{\theta(t;\alpha_{n-2},\alpha_{n-1},\alpha_n)} + \underbrace{\pi \sum_{i=0}^{n-3} h_i \alpha_i}_{\theta_{n-3}} \tag{4}$$

The first term $\theta(t; \alpha_{n-2}, \alpha_{n-1}, \alpha_n)$ defines the phase trajectory during the interval $nT \le t \le (n+1)T$ which is a function of the current symbol α_n and the previous two symbols α_{n-1} and α_{n-2}. The three

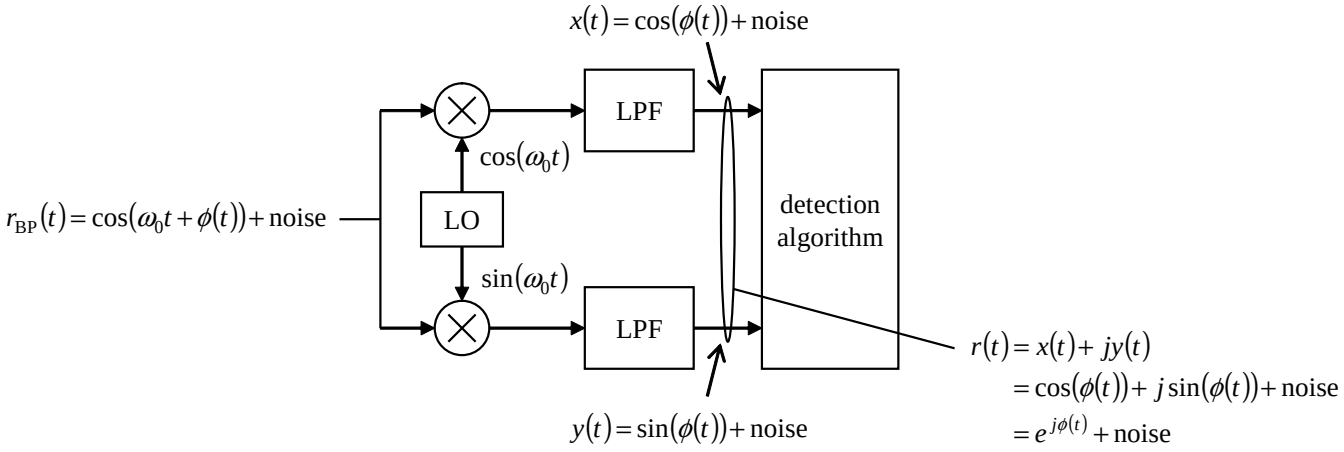

Figure 2: I/Q demodulator and CPM detector.

symbols needed to define the value of this term are called the *correlative state vector*. Since each value of α can have 4 possible values, there are $M^L = 4^3 = 64$ possible trajectories $\theta(t; \alpha_{n-2}, \alpha_{n-1}, \alpha_n)$ can assume. The second term θ_{n-3} is called the *phase state* and represents the contribution to the carrier phase from all symbols that have worked their way through the frequency pulse and now contribute a constant value to the overall carrier phase. Since there are two modulation indexes with values 4/16 and 5/16, it can be shown that θ_{n-3} has 32 possible values $0, \pi/16, 2\pi/16, \cdots, 31\pi/16$.

The phase state and the correlative state vector are all that is required to describe the modulated carrier at any given time. As such, the modulated signal can be thought of as a finite state machine. The role of the receiver is to determine the sequence of inputs to the state machine based on observing noisy waveforms. Note that ARTM CPM requires a different type of detection algorithm than PCM/FM or the ARTM Tier-1 waveforms FQPSK and SOQPSK. This difference is due to the fact that the memory in the waveform makes the performance of symbol-by-symbol detection poor. A detection algorithm with good performance uses this memory to advantage by estimating a sequence of symbols, rather than individual symbols one at a time. The optimum receiver is summarized in the next Section. The complexity is high, but the detection efficiency is good. The performance of this receiver will be baseline for the less complex receivers summarized afterwards.

OPTIMUM DETECTION OF ARTM CPM: A BASELINE FOR COMPARISON

The basic structure of most CPM detectors is illustrated in Figure 2. The received waveform and noise are mixed from IF to baseband in the form of two quadrature components $x(t) = \cos(\phi(t)) +$ noise and $y(t) = \sin(\phi(t)) +$ noise as shown. For notational convenience, the quadrature components $x(t)$ and $y(t)$ are treated as the real and imaginary parts of a complex-valued waveform $r(t) = x(t) + jy(t)$. All of the detection algorithms in this paper operate on the complex baseband waveform $r(t)$.

The optimum detector chooses the sequence $\hat{\boldsymbol{\alpha}} = \hat{\alpha}_0, \hat{\alpha}_1, \ldots$ that minimizes the energy in the difference between the received waveform and one of the possible waveforms. Expressed mathematically, this

rule is

$$\hat{\boldsymbol{\alpha}} = \arg\min_{\boldsymbol{\alpha}} \left\{ \int \left| r(t) - e^{j\phi(t)} \right|^2 dt \right\} \tag{5}$$

where it is understood that $e^{j\phi(t)}$ is the term that depends on the data sequence $\boldsymbol{\alpha} = \alpha_0, \alpha_1, \ldots$. Expanding the right-hand side of this rule and ignoring terms that do not depend on the data produces an alternate, more workable form, for the decision rule:

$$\hat{\boldsymbol{\alpha}} = \arg\max_{\boldsymbol{\alpha}} \left\{ \text{Re} \left[\int r(t) e^{-j\phi(t)} dt \right] \right\}. \tag{6}$$

Conceptually, this detection algorithm operates as follows to produce an estimate for a length-N sequence: List the 4^N possible data sequences. Denote them $\boldsymbol{\alpha}^1, \boldsymbol{\alpha}^2, \ldots, \boldsymbol{\alpha}^{4^N}$. Compute the right-hand-side of (6) for each of the 4^N possible sequences. Set $\hat{\boldsymbol{\alpha}}$ equal to the sequence corresponding to the maximum value obtained in the previous step.

A practical detector cannot use this algorithm for detection. Estimation of a sequence of 10 symbols requires the parallel computation of the right-hand-side of (6) for $4^{10} = 1,048,576$ different sequences. Estimation of 100 symbols requires $4^{100} \approx 1.6 \times 10^{60}$ parallel computations. A 5 Mbit/sec test lasting 30 minutes produces 9 trillion bits which translates into 4.5 trillion 4-ary symbols. The number of parallel computations required for this sequence exceeds the estimate for the number sub-atomic particles in the universe [6]!

The computational complexity can be reduced to manageable levels by performing the sequence estimation sequentially. The argument of the right-hand-side of (6) may be partitioned to produce a recursive form. At time $(n+1)T$, we have

$$\underbrace{\text{Re}\left[\int_0^{(n+1)T} r(t) e^{-j\phi(t)} dt \right]}_{\lambda(n)} = \underbrace{\text{Re}\left[\int_0^{nT} r(t) e^{-j\phi(t)} dt \right]}_{\lambda(n-1)} + \text{Re}\left[\int_{nT}^{(n+1)T} r(t) e^{-j\phi(t)} dt \right]. \tag{7}$$

This equation suggests that the argument of (6) may be computed recursively. That is, the argument during the time interval $nT \le t \le (n+1)T$ may be computed by adding something to the value from the previous interval. The something that is added is may be expressed as

$$\text{Re}\left[\int_{nT}^{(n+1)T} r(t) e^{-j\phi(t)} dt \right] = \text{Re}\left[e^{j\theta_{n-3}} \int_{nT}^{(n+1)T} r(t) e^{\theta(t;\alpha_{n-2},\alpha_{n-1},\alpha_n)} dt \right] \tag{8}$$

where $\theta(t; \alpha_{n-2}, \alpha_{n-1}, \alpha_n)$ is the phase trajectory and θ_{n-3} is the phase state defined in (4). The memory requirements can be reduced by using the Viterbi algorithm [7]. The Viterbi algorithm tracks the 64 possible values of the correlative state vector $\boldsymbol{\alpha}_n = (\alpha_{n-2}, \alpha_{n-1}, \alpha_n)$ and the 32 possible values of the phase state θ_{n-3}. Denote the l-th possible value of the correlative state vector as

$$\boldsymbol{\alpha}_n^l = (\alpha_{n-2}^l, \alpha_{n-1}^l, \alpha_n^l) \quad 0 \le l < 64 \tag{9}$$

and denote the m-th possible value of the phase state as

$$\theta_{n-3}^m = \frac{2\pi}{32} m \quad 0 \le m < 32. \tag{10}$$

The metric corresponding to the l-th value of the correlative state vector and the m-th value of the phase state is

$$\lambda^{l,m}(n) = \lambda^{l,m}(n-1) + \text{Re}\left[e^{-j\theta^m_{n-3}} \int_{nT}^{(n+1)T} r(t) e^{-\theta(t;\alpha^l_{n-2},\alpha^l_{n-1},\alpha^l_n)} dt\right]. \tag{11}$$

The Viterbi algorithm organizes the possible values into a *trellis* connected by *branches*. At each step, the metrics for all possible transitions from all trellis states to all other trellis states are computed and used to update the metrics for each of the paths through the trellis. Only those branches that have a chance of being selected at the end are kept. The others are discarded to reduce the memory requirements.

The algorithm may be organized in hardware as illustrated in Figure 3. The integral expression on the right-hand-side of (11) may be computed using a filter whose impulse response is a time-reversed version of the phase trajectory corresponding to $\boldsymbol{\alpha}^l_n$. Since there are 64 possible correlative state vectors, 64 matched filters are required. These 64 matched filter outputs are combined with the 32 possible phase states to compute all possible values of the last term on the right-hand-side of (11). Note that each branch can be labelled with a *branch vector* of the form

$$\sigma^{l,m}_{2048} = (\theta^m_{n-3}, \alpha^l_{n-2}, \alpha^l_{n-1}, \alpha^l_n). \tag{12}$$

The Viterbi algorithm updates its estimate of the best sequence for each trellis state and stores it. The Viterbi algorithm requires $32 \times 4^2 = 512$ trellis states and $32 \times 4^3 = 2048$ branches.

The number of complex-valued matched filters is 64. The number of real-valued matched filters is $4 \times 64 = 256$. Half of these filters may be eliminated using the symmetry properties $\cos(-x) = \cos(x)$ and $\sin(-x) = -\sin(x)$. Thus the total number of real-valued matched filters of duration T is 128. Note that in addition to the memory and computation requirements of the sequence estimator, the carrier phase offset and symbol timing offset also need to be estimated and tracked.

The complexity of this approach can be prohibitive. In the next section, approximations that reduce the number of trellis states (and, as a consequence, the number of branches) is examined. The loss in detection efficiency due to these approximations is also quantified. The summary demonstrates the complexity/performance trade-off available for ARTM CPM. Afterwards, methods that eliminate the need for carrier phase tracking are summarized and presented.

COHERENT DETECTION

A. Tilted Phase

The first complexity-reducing technique that can be applied is the "tilted phase" technique described in [8]. This method uses a different value, called the tilted phase, in place of the phase state to reduce the number of phase states by 2. The tilted phase values for ARTM CPM are

$$\tilde{\theta}_{n-3} = 0, \frac{2\pi}{16}, \ldots, 15\frac{2\pi}{16} \tag{13}$$

$$\tilde{\theta}^m_{n-3} = \frac{2\pi}{16} m \quad 0 \le m < 16. \tag{14}$$

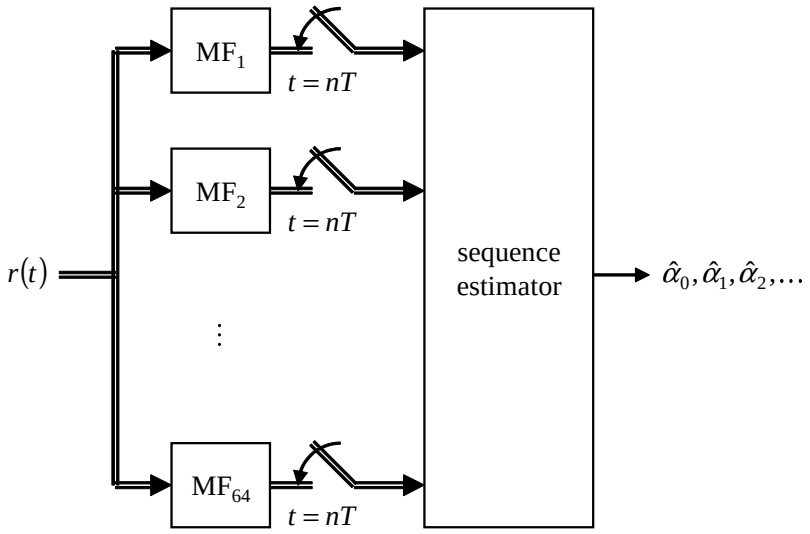

Figure 3: CPM detector showing matched filters and the use of sampled matched filter outputs for sequence detection.

There is no loss in detection efficiency with this technique. By using only 16 phase states, the number of trellis branches is reduced from 2048 to 1024. The branch vector labels in this case are

$$\sigma_{1024}^{l,m} = (\tilde{\theta}_{n-3}^{m}, \alpha_{n-2}^{l}, \alpha_{n-1}^{l}, \alpha_{n}^{l}). \tag{15}$$

The number of matched filters required remains the same.

B. Svensson, Sundberg, & Aulin (SSA) Technique

The frequency pulse in Figure 1 has a time duration equal to 3 symbol times. However, the amplitude of the pulse is very small for $t < 0.5T$ and $t > 2.5T$. The complexity of the trellis can be reduced by approximating the length-$3T$ frequency pulse with a truncated version that has length $2T$. This type of approximation was first proposed in [9] and a nice description can be found in [7, Chapter 8]. This approximation was applied to ARTM CPM in the detector described in [5].

In this case, the phase trajectory $\theta(t; \alpha_{n-2}, \alpha_{n-1}, \alpha_n)$ is now a function of only α_{n-1} and α_n and can be replaced by a new phase trajectory $\tilde{\theta}(t; \alpha_{n-1}, \alpha_n)$. The contribution to the symbol α_{n-2}^{l} is absorbed into the phase state $\tilde{\theta}_{n-2}^{m}$. (Note that the tilted phase is used here.) This reduces the trellis to 64 states, and the number of real-valued matched filters from 128 to 32. The branch vector in this case is

$$\sigma_{256}^{l,m} = (\tilde{\theta}_{n-2}^{m}, \alpha_{n-1}^{l}, \alpha_{n}^{l}), \qquad 0 \le m < 16, \quad 0 \le l < 16 \tag{16}$$

and the metric update equation is

$$\lambda^{l,m}(n) = \lambda^{l,m}(n-1) + \text{Re}\left[e^{-j\tilde{\theta}_{n-2}^{m}} \int_{(n+1/2)T}^{(n+3/2)T} r(t) e^{-\tilde{\theta}(t;\alpha_{n-1}^{l},\alpha_{n}^{l})} dt \right]. \tag{17}$$

The details needed to construct the matched filters are found in [9, 7].

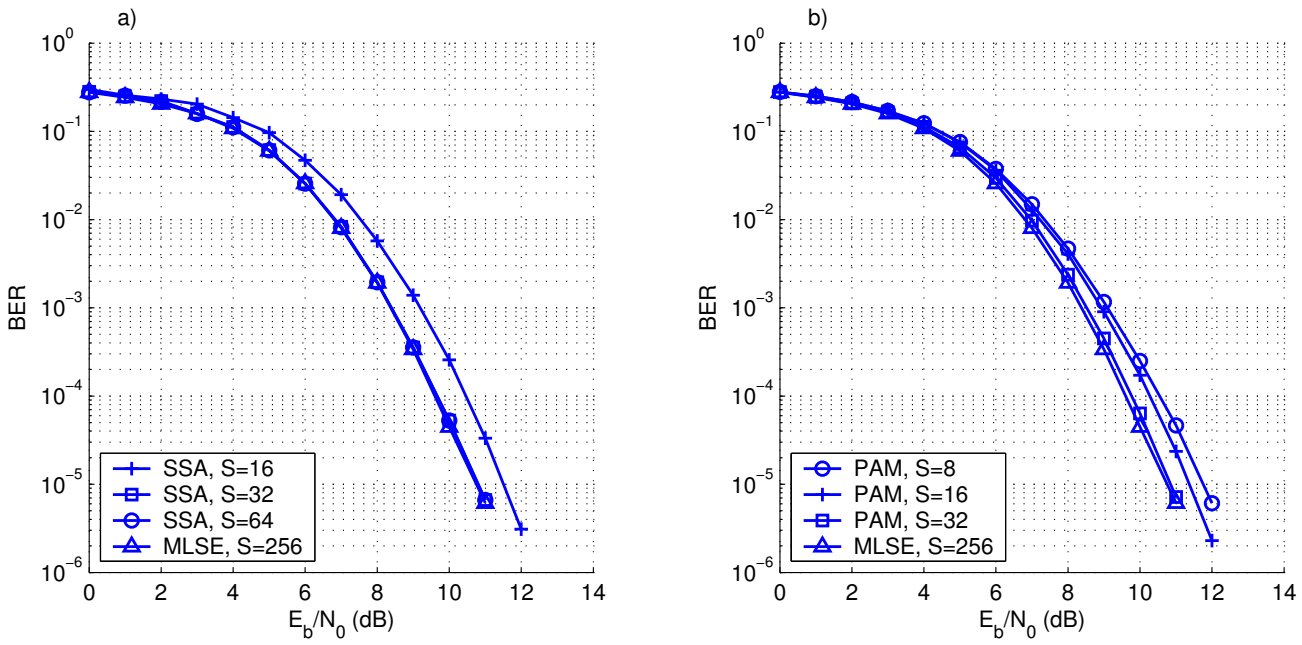

Figure 4: a) Performance of the SSA class of receivers. The 64- and 32-state receivers have near-optimal performance while the 16-state receiver has a loss of 0.8 dB at BER $= 10^{-5}$. b) Performance of the PAM class of receivers. The 32-state receiver has near optimal performance, the 16- and 8-state receivers have respective losses of 0.6 and 1.0 dB at BER $= 10^{-5}$.

There is an additional complexity reduction technique which is available, known as reduced state sequence estimation (RSSE) [10]. The concept behind this approximation is straightforward. When *constructing* the trellis, we proceed as if there are only p' phase states, where $p' \leq 16$, which results in a much smaller trellis. Once the trellis is organized, the branch transitions from state to state are fixed. During receiver *operation* we do not use a fixed number for the phase state, as was the case in (14). Instead, we compute the phase state directly from past decisions $\hat{\alpha}_n$ using an infinite sum as in (4) (the tilted phase technique also used here). More details on RSSE are found in [10]. We label this decision directed phase state as $\hat{\theta}^m_{p',n-3}$. By selecting $p' = 8$ we obtain a 32-state trellis, and with $p' = 4$ we have 16 states. These are specified respectively by the branch vectors

$$\sigma^{l,m}_{128} = (\hat{\theta}^m_{8,n-2}, \alpha^l_{n-1}, \alpha^l_n), \qquad 0 \leq m < 8, \quad 0 \leq l < 16 \tag{18}$$

$$\sigma^{l,m}_{64} = (\hat{\theta}^m_{4,n-2}, \alpha^l_{n-1}, \alpha^l_n), \qquad 0 \leq m < 4, \quad 0 \leq l < 16. \tag{19}$$

The performance of this class of receivers is shown in Figure 4 (a) where we note that the 64- and 32-state receivers have identical performance, which is also nearly identical to the optimal 256-state receiver. The nearly 0.8 dB lost by the 16-state receiver is a result of suboptimal *merges* which are created by the highly reduced trellis. A more detailed analysis of this merge behavior is given in [11].

C. *Pulse Amplitude Modulation (PAM) Technique*

An entirely different viewpoint for CPM is given by the PAM representation, which was first derived for binary single-h CPM by Laruent [12] and later extended to M-ary single-h CPM by Mengali and Morelli [13] and to M-ary multi-h CPM by Perrins and Rice [14, 15]. Using the PAM representation, the ARTM CPM waveform may be expressed as

$$e^{j\phi(t)} = \sum_{k=0}^{47} \sum_{n} a_{k,n} g_{k,\underline{n}}(t - nT) \tag{20}$$

where $\{a_{k,n}\}$ is a set of 48 *pseudo-symbols* which modulate the amplitude of the signal pulses $g_{k,\underline{n}}(t)$. The details required to construct the pseudo-symbols and signal pulses are too numerous to give here, a full description is available in [15]. The essential characteristics of these quantities are: 1) the signal pulses vary in amplitude and duration, 2) the longest pulses (of duration $3T$ and $4T$) have the largest amplitude while the shortest pulses (of duration T) have extremely small amplitude, 3) the set of 48 pseudo-symbols can be represented by a 256-state trellis (using the tilded phase) with the branch vector (15), and 4) within the set of 48 pseudo-symbols, the ones associated with the largest pulses do not require a full 256-state trellis.

These characteristics are exploited to produce a detector based on a set of 3 averaged pulses, $\overline{g}_0(t)$, $\overline{g}_1(t)$, and $\overline{g}_2(t)$, and a trellis with only 64 states [16]. The trellis branches are labeled by the branch vector (15). Additional complexity reduction is again available via RSSE, which results in the same branch vectors as before for the 32- and 16-state configurations, (18) and (19) respectively. We can also apply RSSE to replace the *hypothesized* symbol α_{n-1}^{l} with the *decision* $\hat{\alpha}_{n-1}^{l}$, which produces an 8-state trellis with the branch vector

$$\sigma_{32}^{l,m} = (\hat{\theta}_{8,n-2}^{m}, \hat{\alpha}_{n-1}^{l}, \alpha_{n}^{l}), \qquad 0 \le m < 8, \quad 0 \le l < 4. \tag{21}$$

The reason this last approximation is available here, but not in the SSA case, is that the PAM receiver metrics accumulate distance in a fundamentally different manner that allows much more aggressive use of RSSE [11].

The PAM receiver metrics are

$$\lambda^{l,m}(n) = \lambda^{l,m}(n-1) + \mathrm{Re}\left[\sum_{k=0}^{2} (b_{k,\underline{n}}^{l,m})^{*} \int_{nT}^{(n+D_k)T} r(t)\overline{g}_k(t - nT)dt\right] - S^{l,m} \tag{22}$$

where D_k is the length (in symbol times) of pulse $\overline{g}_k(t)$, $\{b_{k,\underline{n}}^{l,m}\}$ is the set of 3 pseudo-symbols which are derived from the original pseudo symbols $\{a_{k,\underline{n}}^{l,m}\}$ by some averaging steps, and $S^{l,m}$ is a bias constant associated with each branch [16]. This receiver metric is an approximation of the optimal metric (11). However note that if the original set of 48 pulses in (20) is used in (22), it is equivalent to the optimal metric (11) and constitutes an alternate optimum configuration.

The performance of the PAM class of receivers is shown in Figure 4 (b), where the 32-state receiver is within a tenth of a dB of the optimum. At BER $= 10^{-5}$, the 16-state receiver is within 0.6 dB of the

optimum, while the 8-state receiver is within 1.0 dB. For the 16-state case, this is a slight improvement over the 16-state SSA receiver. Another important comparison between these two reduced-complexity coherent approaches is the computational requirements for the matched filtering. For the SSA technique, 32 length-T real-valued matched filters were required. For the PAM technique, the 3 matched filters are real with lengths $4T$, $3T$, and $2T$. This corresponds to 18 length-T real-valued filters, or nearly half as many as in the SSA case.

NONCOHERENT DETECTION

We now turn our attention to noncoherent detection techniques. In this setting, the receiver requires no knowledge of the channel phase. However, most noncoherent techniques (including the ones presented here) assume the channel phase is slowly varying such that it can be regarded as constant over a brief period of time. Noncoherent detection does not estimate or track the channel phase and uses the decision rule

$$\hat{\boldsymbol{\alpha}} = \arg\max_{\boldsymbol{\alpha}} \left\{ \left| \int r(t) e^{-j\phi(t)} dt \right|^2 \right\}. \tag{23}$$

We note that the decision rules (6) and (23) are identical except that the coherent receiver takes the real part of the correlation and the noncoherent receiver takes the magnitude-squared of the correlation.

We now consider three noncoherent detection schemes which are motivated by (23). These different schemes all use the original bank of 128 matched filters that were used for the optimum receiver. An important difference in the noncoherent case is that the phase state, with its infinitely long sum, is useless in the decision rule (23) due to the magnitude-squared operation, as explained in [17]. In order to approximate the phase state, the *rotational state vector* $\boldsymbol{\beta}_n^r$ is used, which is defined as

$$\boldsymbol{\beta}_n^r = (\alpha_{n-N-1}^r, \alpha_{n-N}^r, \cdots, \alpha_{n-3}^r), \qquad 0 \le r < 4^{N-1} \tag{24}$$

where the variable length of the rotational state vector is parameterized by the integer $N > 0$. The rotational state vector is associated with a *branch phase* $\Omega(\boldsymbol{\beta}_n^r)$ which is given by

$$\Omega(\boldsymbol{\beta}_n^r) = \left(\pi \sum_{k=n-N-1}^{n-3} \alpha_k^r h_{\underline{k}} \right) \bmod 2\pi. \tag{25}$$

The overall hypothesis is given by the branch vector

$$\sigma_N^{l,r} = (\boldsymbol{\beta}_n^r, \alpha_{n-2}^l, \alpha_{n-1}^l, \alpha_n^l), \qquad 0 \le r < 4^{N-1}, \quad 0 \le l < 64 \tag{26}$$

where each branch in the trellis is associated with an (l, r) pair and the trellis has $S = 4^{N+1}$ states. We note that this trellis has only a finite hypothesis, since we have removed the phase state and replaced it with the $N-1$ symbol coordinates in $\boldsymbol{\beta}_n^r$. We also observe that as N increases, the branch phase (25) approximates the phase state in (4), at the expense of exponentially increasing complexity.

A. *Aulin & Sundberg Technique*

The receiver in [18] computes the decision rule (23) exactly, but only over a limited time interval. If we let $N_1 + N_2 - 1 = N$, then the receiver metric is

$$\lambda^{l,r}(n) = \sum_{k=n-N_1+1}^{n+N_2} e^{-j\Omega(\boldsymbol{\beta}_k^r)} \int_{kT}^{(k+1)T} r(t) e^{-j\theta(t;\alpha_{n-2}^l,\alpha_{n-1}^l,\alpha_n^l)} dt \tag{27}$$

$$\begin{aligned} &= \lambda^{l,r}(n-1) + e^{-j\Omega(\boldsymbol{\beta}_{n+N_2}^r)} \int_{(n+N_2)T}^{(n+N_2+1)T} r(t) e^{-j\theta(t;\alpha_{n-2}^l,\alpha_{n-1}^l,\alpha_n^l)} dt \\ &\quad - e^{-j\Omega(\boldsymbol{\beta}_{n-N_1}^r)} \int_{(n-N_1)T}^{(n-N_1+1)T} r(t) e^{-j\theta(t;\alpha_{n-2}^l,\alpha_{n-1}^l,\alpha_n^l)} dt \end{aligned} \tag{28}$$

which is simply the sum of N consecutive matched filter outputs each rotated by the proper branch phase such that they add constructively along the phase trajectory of the hypothesis. The matched filter outputs are taken from the sliding observation window $(n-N_1+1)T \le t \le (n+N_2+1)T$. There is no traceback operation here; the receiver simply computes the complex-valued metrics for each branch, selects the survivor at each merging node with the largest metric (in the magnitude-squared sense), and outputs the symbol $\hat{\alpha}_n$ corresponding to the hypothesis which maximizes (28) over all the states. There is an implied delay of N_2 needed in order to compute these metrics. This architecture was first derived for binary continuous phase frequency shift keying (CPFSK) in [19], and has been implemented for PCM/FM with much success in [20]. However, for the case of ARTM CPM, the simulations will show that a large (impractical) value of N is required to achieve satisfactory performance. A potentially large value of N is consistent with the findings of the performance analysis in [18].

B. *Colavolpe & Raheli Technique*

The noncoherent receiver metrics in [21] are obtained by expanding the magnitude-squared expression on the right-hand-side of (23) and keeping only those terms which are relevant to the hypothesis. The recursive form of the metric is

$$\begin{aligned} \lambda^{l,r}(n) = \lambda^{l,r}(n-1) + \mathrm{Re}\Bigg[&\sum_{k=1}^{N-1} e^{-j\Omega(\boldsymbol{\beta}_n^r)} \int_{nT}^{(n+1)T} r(t) e^{-j\theta(t;\alpha_{n-2}^l,\alpha_{n-1}^l,\alpha_n^l)} dt \\ &\times \left(e^{-j\Omega(\boldsymbol{\beta}_{n-k}^r)} \int_{(n-k)T}^{(n-k+1)T} r(t) e^{-j\theta(t;\alpha_{n-k-2}^l,\alpha_{n-k-1}^l,\alpha_{n-k}^l)} dt \right)^* \Bigg] \end{aligned} \tag{29}$$

which is an approximation of the exact decision rule (23). We note that the presentation in [21] uses matched filters which are based on the pulse amplitude modulation (PAM) representation of CPM [12, 13] and are not the same as those matched to the phase trajectory as used in (29). For the purposes of our discussion, the metric (29) is still valid. However the PAM representation does result in additional complexity savings. The real-valued metric increment in (29) is simply the most recent matched filter output correlated against the $N-1$ previous matched filter outputs (all of the matched filter outputs are

phase-rotated by the branch phase in order to be consistent with the particular hypothesis). This receiver uses a traditional traceback operation. Also, since (29) is real-valued, there is no magnitude-squared operation required in determining the survivors at each merging node. There is no analysis that describes the performance of this receiver. However, the simulations for 4-ary partial response CPM with $L = 2$ and $h = 1/4$ in [21] show that near-optimal performance can be achieved with $N \approx 5$.

C. Perrins & Rice Technique

The third noncoherent technique was first applied to ARTM CPM in [22], with a more general treatment (including performance analysis) given in [17]. The complex-valued receiver metric is

$$\lambda^{l,r}(n) = a\lambda^{l,r}(n-1) + e^{-j(\Omega(\boldsymbol{\beta}_n^r)+\hat{\theta}_n^{l,r})} \int_{nT}^{(n+1)T} r(t) e^{-j\theta(t;\alpha_{n-2}^l,\alpha_{n-1}^l,\alpha_n^l)} dt \tag{30}$$

which is similar to the recursive metric (11) of the optimal coherent receiver. The branch metric increments are simply the sampled matched filter output rotated by a certain phase such that it is consistent with the ongoing hypothesis of the particular trellis path. However, the *leakage factor* a, $0 \leq a < 1$, causes the cumulative metric $\lambda^{l,r}(n)$ to be a leaky integral with limited memory. When the leakage factor is close to unity, the receiver can obtain near optimal performance when degradations such as the time-varying channel phase and phase noise are ignored. When the leakage factor is reduced, the receiver becomes more robust under such conditions at the expense of an increasing loss in overall performance [17]. The phase rotation in (30) is divided into two parts, the branch phase in (25) and the *cumulative phase* $\hat{\theta}_n^{l,r}$, which is given by

$$\hat{\theta}_n^{l,r} = \left(\pi \sum_{k=-\infty}^{n-L-N+1} \hat{\alpha}_k^{l,r} h_{\underline{k}} \right) \bmod 2\pi. \tag{31}$$

This cumulative phase is not composed of *hypothesized* data symbols; instead, it is the phase contribution of the history of past *decisions*, $\hat{\alpha}_k^{l,r}$, that have been made in the trellis. Each state in the trellis maintains a value for the cumulative phase (just as they also maintain a cumulative metric) and it is updated recursively and propagated with the surviving metric at each merging node. The branch metrics in (30) propagate from state to state as complex numbers. However, when competing metrics are compared to each other at merges, the survivor is the one with the largest magnitude squared, as indicated by (23).

D. Limiter-Discriminator Detection

A fourth noncoherent detection method, one which is not motivated by the decision rule (23), is limiter discriminator detection [23]. This method, illustrated by the block diagram in Figure 5, is the current method used for detecting PCM/FM. The received signal is band-pass filtered and demodulated using a traditional limiter-discriminator. The output, $d\phi(t)/dt$, is processed by a sequence detector in the form of a modified bit synchronizer. The sequence detector is based on the Viterbi algorithm, which uses the outputs of a bank of filters matched to the to the combined response of the bandpass filter and the time derivative of the phase trajectory $d\theta(t;\alpha_{n-2},\alpha_{n-1},\alpha_n)/dt$ when no noise is present [23]. This receiver requires $S = 4^{L_{\text{IF}}+2}$ states and $4^{L_{\text{IF}}+3}/2$ real-valued matched filters, where L_{IF} is the length of the impulse response

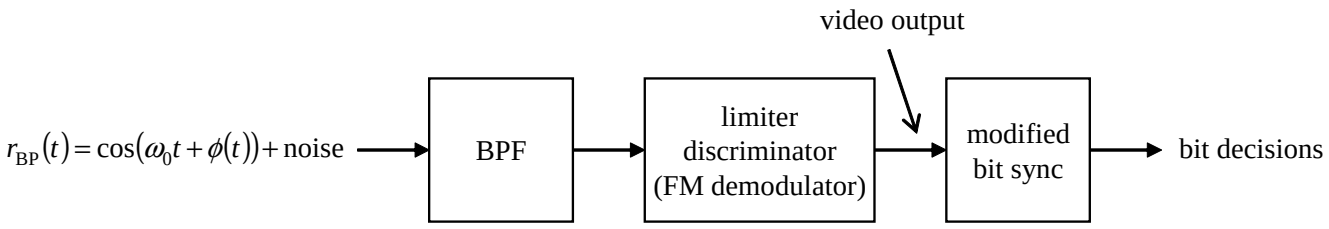

Figure 5: Using a limiter-discriminator for detection of ARTM CPM.

of the bandpass filter (in symbol times). The complexity of this receiver turns out to be somewhat high in return for relatively poor performance, as the simulations will show. However, there is some investigation that could be done to make the matched filters independent of the data, which would drastically reduce the required number of matched filters.

E. Simulation Results for Noncoherent Techniques

The simulated performance of these four noncoherent detection schemes is shown in Figure 6. In terms of performance, the two most viable techniques are Colavolpe & Raheli and Perrins & Rice. Using BER $= 10^{-5}$ as a reference point, these two receivers have respective losses of 1.6 and 1.9 dB relative to MLSE. In terms of state complexity, the Perrins & Rice receiver has a large advantage with only $S = 64$ states. The Colavolpe & Raheli receiver requires $S = 1024$ to outperform the low-complexity Perrins & Rice receiver. It might be possible to reduce the number of states by a factor of 4 with little or no performance loss using the PAM decomposition; however, these PAM simplifications are also available for the Perrins & Rice receiver, so the relative difference in complexity would likely remain unchanged. For the Perrins & Rice receiver, selecting $N = 3$ improves performance by a few tenths of a dB, with a 4-fold increase in the number of states; additional increments of N bring diminishing performance gains.

The limiter-discriminator technique has a loss of 6 dB relative to MLSE at BER $= 10^{-5}$. The Aulin & Sundberg technique is not well suited for this application, since an $S = 4096$ configuration is not even able to attain BER $= 10^{-5}$ for the range of E_b/N_0 values considered in the simulations. This is not the case for PCM/FM, where the Aulin & Sundberg receiver performs very well with modest complexity of $S = 32$ [20].

SUMMARY AND CONCLUSIONS

In this paper we have surveyed the available coherent and noncoherent detection techniques for ARTM CPM. The results of this survey are summarized in Table 2. For coherent detection, we have shown that the full 256-state optimal implementation is not necessary to achieve satisfactory performance; two different 32-state configurations were found to perform within one tenth of a dB of optimal. For noncoherent detection, the state complexity is controlled by the parameter N and can be quite large in some cases. One noncoherent technique performed within 1.9 dB of the optimal with only 64 states, which is significant when considering the additional complexity savings of not having to track the carrier phase.

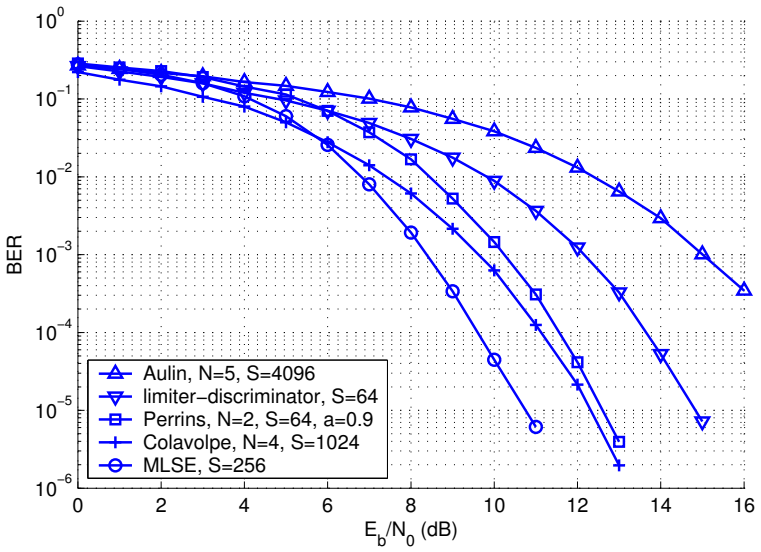

Figure 6: Performance of the four noncoherent detection schemes relative to the optimal MLSE receiver. At BER $= 10^{-5}$, the Colavolpe & Raheli and Perrins & Rice techniques perform the best with losses of only 1.6 and 1.9 dB, respectively. The losses for the limiter-discriminator and Aulin & Sundberg techniques are much larger.

Table 2: Summary of the detection efficiency and complexity of the receivers surveyed in this paper. The number of matched filters is the equivalent number of real-valued filters of length T.

detector	number of matched filters	number of states	number of branches	E_b/N_0 required for BER $= 10^{-5}$	carrier phase sync required	timing sync required
optimum	128	512	2048	10.75 dB	Y	Y
titled phase	128	256	1024	10.75 dB	Y	Y
SSA	32	64	256	10.80 dB	Y	Y
SSA + RSSE	32	32	128	10.80 dB	Y	Y
SSA + RSSE	32	16	64	11.50 dB	Y	Y
PAM + RSSE	18	32	128	10.85 dB	Y	Y
PAM + RSSE	18	16	64	11.37 dB	Y	Y
PAM + RSSE	18	8	32	11.76 dB	Y	Y
Colavolpe $N = 4$	128	1024	4096	12.32 dB	N	Y
Perrins $N = 4$, $a = 0.9$	128	64	256	12.65 dB	N	Y
Limiter-Discriminator	32	64	256	14.84 dB	N	Y
Aulin $N = 5$	128	4096	16384	~ 19 dB	N	Y

REFERENCES

[1] C. Irving. Range telemetry improvement and modernization. In *Proceedings of the International Telemetering Conference*, pages 294 – 303, Las Vegas, NV, October 1997.

[2] W. Gao and K. Feher. FQPSK: A bandwidth and RF power efficient technology for telemetry applications. In *Proceedings of the International Telemetering Conference*, Las Vegas, NV, October 1997.

[3] T. Hill. An enhanced, constant envelope, interoperable shaped offset QPSK (SOQPSK) waveform for improved spectral efficiency. In *Proceedings of the International Telemetering Conference*, pages 127–136, San Diego, CA, October 2000.

[4] E. Law and K. Feher. FQPSK versus PCM/FM for aeronautical telemetry applications; spectral occupancy and bit error probability comparisons. In *Proceedings of the International Telemetering Conference*, pages 489–496, Las Vegas, NV, October 1997.

[5] M. Geoghegan. Description and performance results for the advanced range telemetry (ARTM) Tier II waveform. In *Proceedings of the International Telemetering Conference*, San Diego, CA, October 2000.

[6] S. Hawking. *Black Holes and Baby Universes and Other Essays*. Bantam Books, 1993.

[7] J. B. Anderson, T. Aulin, C-E. Sundberg. *Digital Phase Modulation*. Plenum Press, New York, 1986.

[8] B. E. Rimoldi. "A decomposition approach to CPM". *IEEE Trans. Info. Theory*, 34:260–270, March 1988.

[9] A. Svensson, C-E. Sundberg, and T. Aulin. "A class of reduced-complexity Viterbi detectors for partial response continuous phase modulation". *IEEE Trans. Commun.*, 32:1079–1087, Oct. 1984.

[10] A. Svensson. "Reduced state sequence detection of partial response continuous phase modulation". *IEE Proc., pt. I*, 138:256–268, Aug. 1991.

[11] E. Perrins and M. Rice. Unified performance analysis of suboptimum detection methods for multi-h CPM. In *Proceedings of the IEEE Military Communications Conference*, Monterey, CA, October 2004.

[12] P. A. Laurent. "Exact and approximate construction of digital phase modulations by superposition of amplitude modulated pulses (AMP)". *IEEE Trans. Commun.*, 34:150–160, February 1986.

[13] U. Mengali and M. Morelli. "Decomposition of M-ary CPM signals into PAM waveforms". *IEEE Trans. Info. Theory*, 41:1265–1275, Sept. 1995.

[14] E. Perrins and M. Rice. "A linear PAM-based receiver for multi-h CPM". In *Proceedings of the International Telemetering Conference*, Las Vegas, NV, October 2003.

[15] E. Perrins and M. Rice. "PAM decomposition of M-ary multi-h CPM". *IEEE Transactions on Communications*, in review, September 2003.

[16] E. Perrins and M. Rice. "Optimal and reduced complexity receivers for M-ary multi-h CPM". In *Proceedings of the IEEE Wireless Communications and Networking Conference, WCNC'04*, Atlanta, Georgia, March 2004.

[17] E. Perrins and M. Rice. "On noncoherent detection of CPM". Submitted to *IEEE Journal on Selected Areas in Communications*, April 2004.

[18] T. Aulin and C-E. Sundberg. "Partially coherent detection of digital full response continuous phase modulated signals". *IEEE Transactions on Communications*, 30(5):1096–1117, May 1982.

[19] W. P. Osborne and M. B. Luntz. "Coherent and noncoherent detection of CPFSK". *IEEE Transactions on Communications*, 22(8):1023–1036, August 1974.

[20] M. Geoghegan. "Improving the detection efficency of conventional PCM/FM telemetry by using a multi-symbol demodulator". In *Proceedings of the International Telemetering Conference*, San Diego, CA, October 2000.

[21] G. Colavolpe and R. Raheli. "Noncoherent sequence detection of continuous phase modulations". *IEEE Transactions on Communications*, 47(9):1303–1307, September 1999.

[22] E. Perrins and M. Rice. "Multi-symbol noncoherent detection of multi-h CPM". In *Proceedings of the International Telemetering Conference*, Las Vegas, NV, October 2003.

[23] E. Perrins and M. Rice. "Comparison of receivers for multi-h CPM". In *Proceedings of the International Telemetering Conference*, San Diego, CA, October 2002.